Geophysical Research Letters

Supporting Information for

Future changes in tropical cyclone activity in high-resolution large-ensemble simulations

Kohei Yoshida[1], Masato Sugi[1], Ryo Mizuta[1], Hiroyuki Murakami[2,1], Masayoshi Ishii[1]

[1]Meteorological Research Institute, Tsukuba, Ibaraki 305-0052, Japan

[2]Geophysical Fluid Dynamics Laboratory, Princeton, NJ 08540-6649, USA

Contents of this file

Introduction

This support information contains additional text, figures, and table to supplement main contents.

Text S1 describes detailed experimental design of the d4PDF data set. See Mizuta et al. [2016] for complete description of the experimental design.

Figure S1 shows the six patterns of SST warming from past to future simulations, together with the multi-model mean pattern and model spread. The tropical mean SST warming ranges from +2.8 to +3.0 K (Figures S1a and c-f). In the multi-model mean, warming in the Northern Hemisphere is larger than in the Southern Hemisphere, and large warming occurs in the equatorial eastern Pacific and Atlantic (Figure S1a). The

spread among the six patterns is large in the Pacific and Atlantic Oceans, and smaller in the NIO (Figure S1b). Each SST warming pattern has its warming peak in a different region of the tropics. The CCSM4-warming has its peak in the equatorial western Pacific (a La Niña or flat pattern), in which the spatial variance of SST increases in the tropics because of the enhanced longitudinal SST gradient. MRI-CGCM3-warming has its peak in the equatorial central Pacific, and the others have their peaks in the equatorial eastern Pacific (shaped like El Niño), in which the spatial variance generally reduces in the future climate. Therefore, these SST warming patterns have distinctive structures and can include better estimates of the uncertainty compared with previous studies [*Murakami et al.*, 2012; *Mizuta et al.*, 2014].

Figure S2 shows relative probabilities of annual TC genesis frequency in each ocean basin. TC genesis frequency in the past climate simulations generally reproduces the observations, but underestimates in ENP and NAT. As shown in Figure 1, all-member simulations have smooth probability distributions, while the probability distributions of a single-member simulation and the observations are not smooth. The mean future reduction rate of TC genesis frequency is significantly large especially in WNP, SIO, and SPA, but quite small in ENP (see also Figure 4). In each ocean basin, the rate of future change relative to the interannual variability is smaller than for the global ocean. The interannual variations of the number of regional TCs have complement relationships in individual oceans, and the interannual variations of global TC genesis frequency consequently shrinks. In individual ocean basins, especially in NIO, ENP, and NAT, the nonparametric probability distributions tend not to match with the estimated normal distributions, comparing with that in the global ocean.

Figure S3 shows future changes in vertical velocity at 500 hPa and vertical wind shear of horizontal wind between 850 and 200 hPa. Both of the vertical wind and vertical shear of horizontal wind have similar distributions to those shown in *Murakami et al.*

[2012a; 2012b]. Future changes in atmospheric circulations such as vertical shear of horizontal wind and vertical wind tend to correspond to CAT45 TC occurrence changes consistent with previous studies. In areas from Hawaii to south of Japan, there appears both increasing vertical velocity and weakening vertical shear of horizontal wind.

Figure S4 and Table S1 show future changes in the four major metrics of TC activity together with uncertainty ranges for each SST warming pattern. We can see large uncertainty ranges in the changes in the metrics in individual ocean basins. The changes in the TC activity metrics in individual ocean basins significantly depend on the prescribed SST warming patterns, especially in ENP and NAT. The TC genesis frequency increases with the MIROC5 SST pattern (+15% to +40% in ENP; +25% to +52% in NAT), but decreases for CCSM4 (‐45% to ‐26% in ENP; ‐59% to ‐37% in NAT). The number of CAT45 drastically increases with the MIROC5 SST (+163 to +307% in ENP; +175% to +275% in NAT), but decreases or slightly increases for CCSM4 (‐62% to +6% in ENP; ‐83% to ‐17% in NAT). The lifetime maximum intensity of surface wind and mean precipitation rate have similar tendency, but the spread of the changes originated by uncertainty of SST warming pattern is smaller. The difference in changes in TC metrics is associated with changes in the SST contrast between the western Pacific and Atlantic in the tropics. While SST warming is relatively high in the tropics of ENP and NAT and low in western and central Pacific in MIROC5, it is high in the WNP and low in ENP and NAT in CCSM4 (Figure S4c and S4f). Additionally, in SPA and WNP, SST warming difference between MIROC5 and MRI-CGCM3 clearly affect the difference in changes in TC activity metrics (Figure S4f and S4h). Relative magnitude of SST warming among individual ocean basins differs in each SST warming pattern, and the difference in SST warming pattern induces the uncertainty of changes in

TC activity metrics through the relationship between regional SST warming and changes in TC metrics as discussed in *Knutson et al.* [2015].

Text S1.

We use the large ensemble simulation data set for current and future climates, d4PDF, which is produced by MRI-AGCM3.2H. The model is based on a numerical weather prediction model of the Japan Meteorological Agency, and is configured for research use [*Mizuta et al.*, 2012]. The horizontal resolution is TL319 (equivalent to a 60-km horizontal grid), there are 64 vertical layers, and the model top is set at 0.01 hPa. MRI-AGCM3.2H is able to reproduce realistic TC activity apart from its intensity [*Murakami et al.*, 2012b]. The current climate simulations were integrated for 60 years from 1951 to 2010 with observed SSTs and sea ice concentration from COBE-SST2 [*Hirahara et al.*, 2014] and observed global warming gas concentrations. The current climate simulations were constituted by 100 ensemble members based on initial value perturbations of the atmosphere and short-term monthly SST perturbations. The magnitude of the monthly SST perturbations is 30% of observed interannual SST variations, which is typical SST analysis errors for recent decades. The future climate simulations were performed for 60 years with a constant warming condition roughly corresponding to the level of year 2090 in the Representative Concentration Pathway 8.5 (RCP8.5) scenario adopted in CMIP5. Because of the large variety in future SST projections, we chose six SST warming patterns projected by six coupled models: CCSM4, GFDL-CM3, HadGEM2-AO, MIROC5, MPI-ESM-MR, and MRI-CGCM3 (see Figure S1). Each SST warming pattern of the RCP8.5 scenario was the difference between SST climatologies of 1991-2010 and 2080-2099 for each month, and then the climatological difference was scaled by a multiplier, so that MRI-AGCM3.2H reproduces 4 K surface air warming from the pre-industrial level. Here, the future monthly SSTs were constructed from adding the SST warming patterns to detrended monthly COBE-SST2 from 1951 to 2010. The future climate simulations were constituted by 90 ensemble members based on the six future

SST patterns, initial value perturbations of the atmosphere, and short-term monthly SST perturbations. For each of six SST warming patterns, 15 ensemble experiments were performed with the perturbations of both initial values of the atmosphere and SST mentioned above. See *Mizuta et al.* [2016] for complete description of the experimental design. Note that the future SSTs used in the present study do not have long-term warming trends for the 60-year integration period.

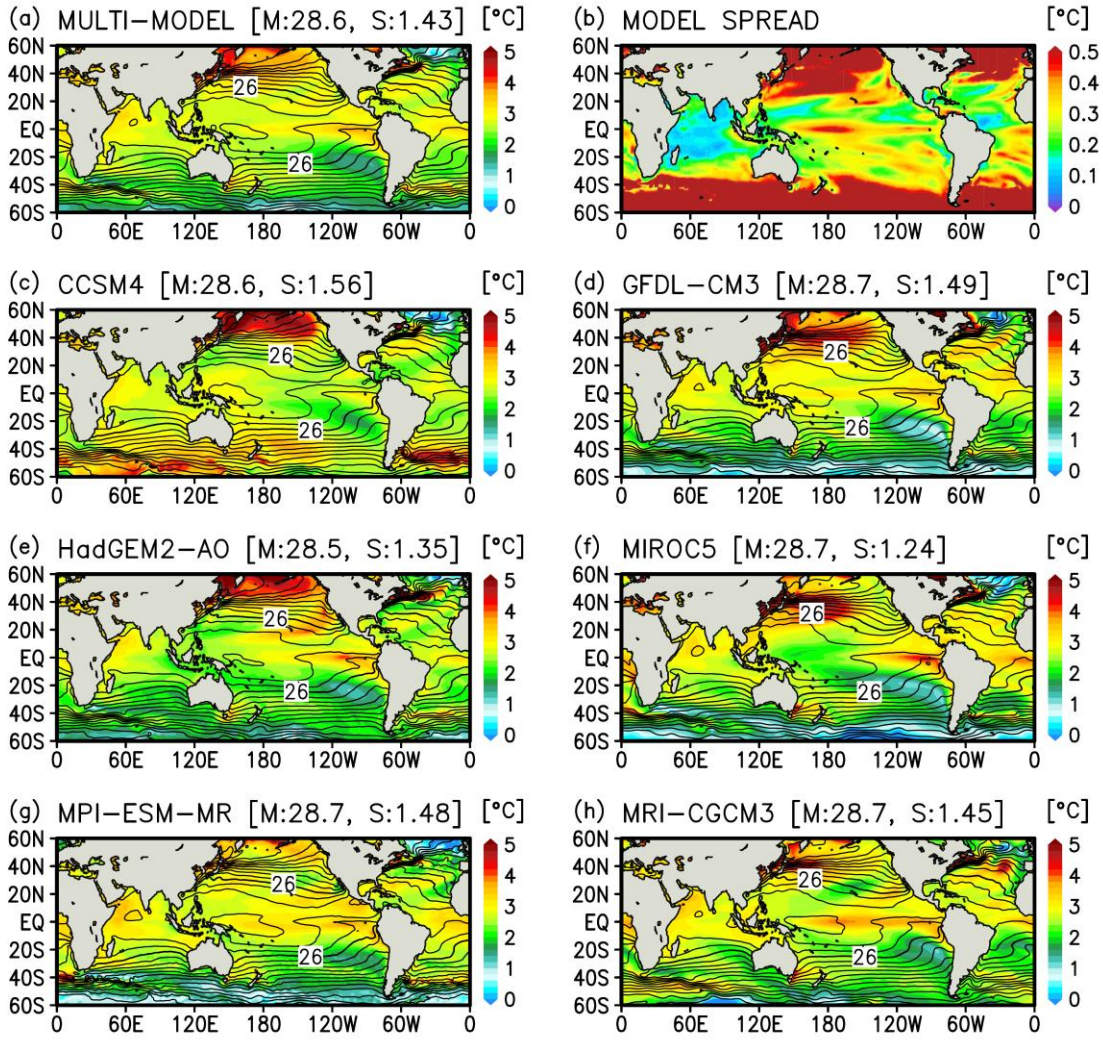

Figure S1. Annual mean prescribed sea surface temperatures (SST; contours) and their future changes (color). Contour intervals are 1°C. (a) multi-model mean SST warming pattern from the six CMIP5 models, (b) standard deviation of SST warming among the six models, (c–h) SST warmings of the six models. The values at the top of each panel indicate tropical-mean (30°S–30°N) SST (M) and spatial standard deviation of SST in the deep-tropics (10°S–10°N) (S).

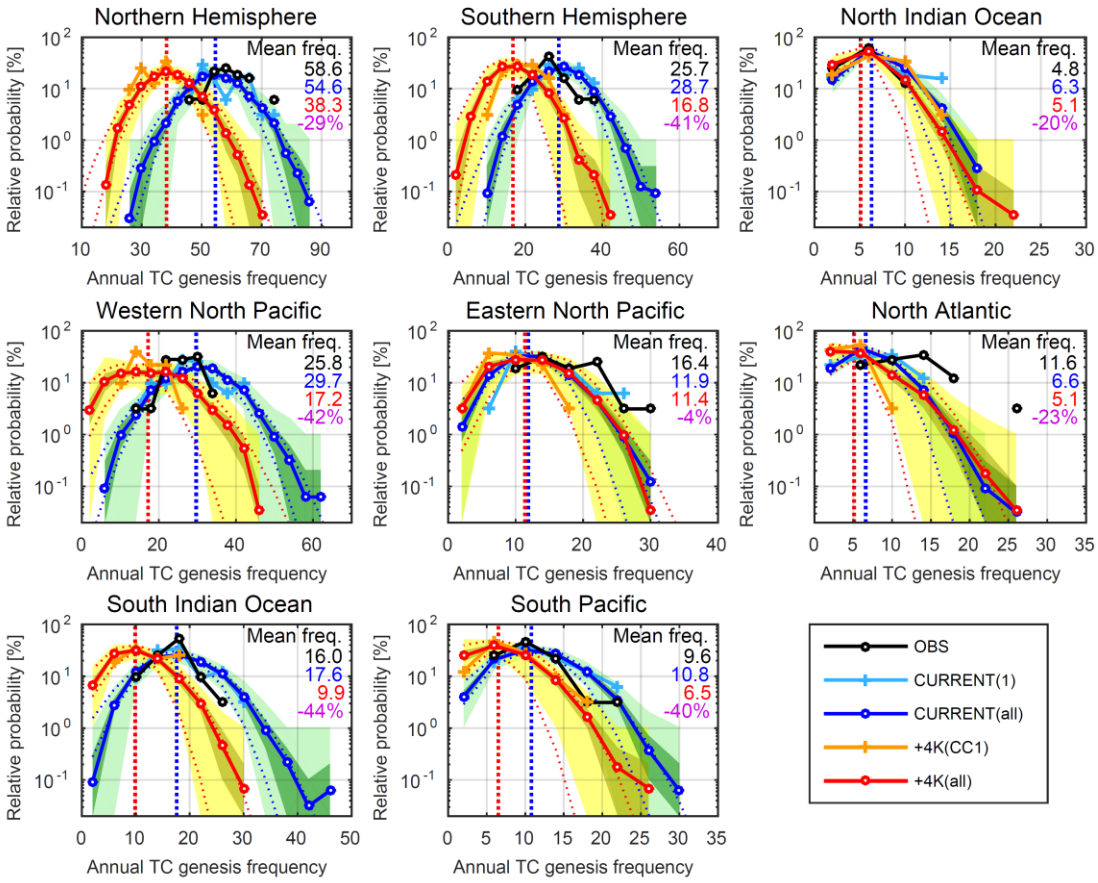

Figure S2. Same as Figure 1 but for the two hemispheres and each ocean basin.

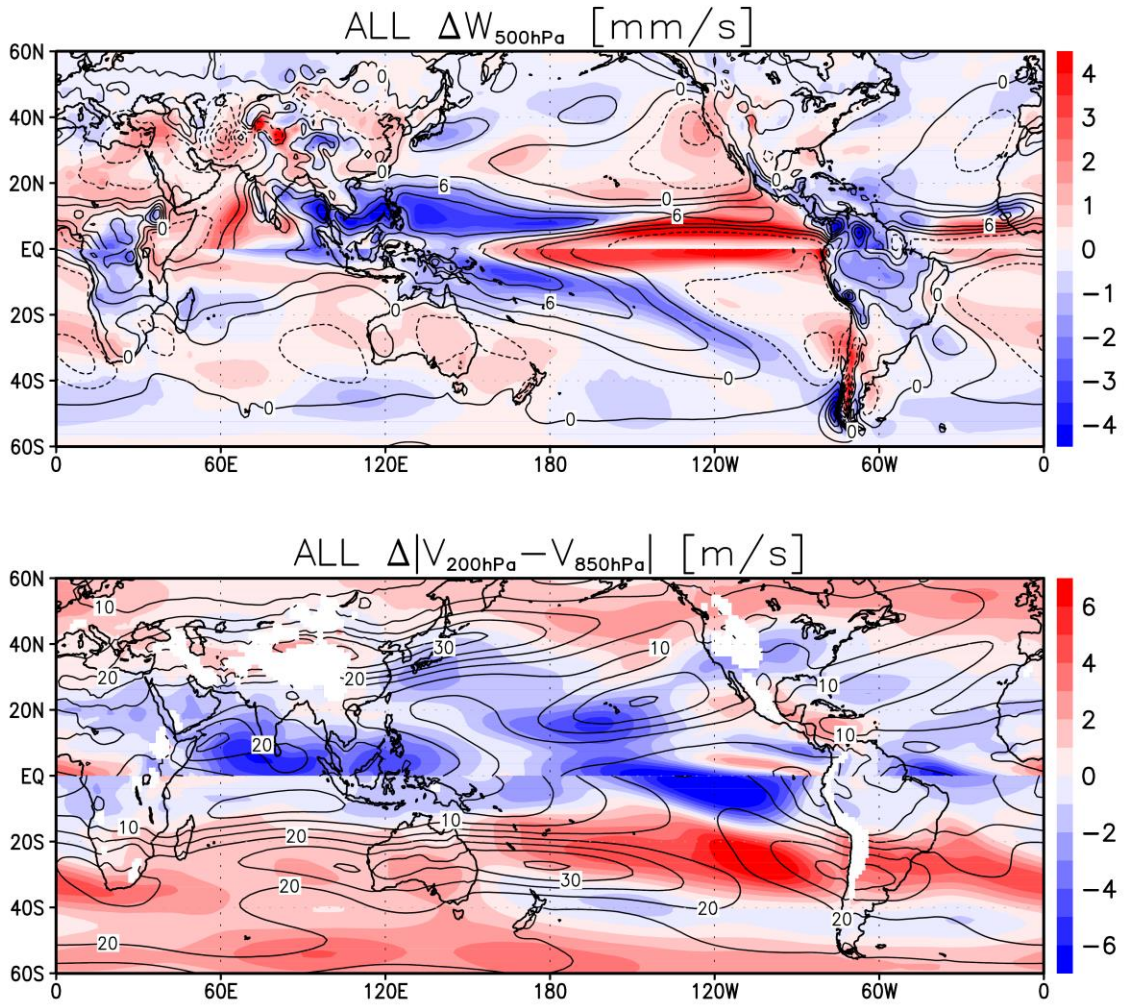

Figure S3. Future changes in climatologies of (top) vertical velocity at 500 hPa [mm/s] and (bottom) vertical shear of horizontal wind between 200 and 850 hPa [m/s]. Contours indicate the values in all-member ensemble mean of current climate simulations, and color shadings indicate difference between values in all-member ensemble mean of the future and current climate simulations. The average from July to October is used in Northern Hemisphere and that from January to April is used in Southern Hemisphere.

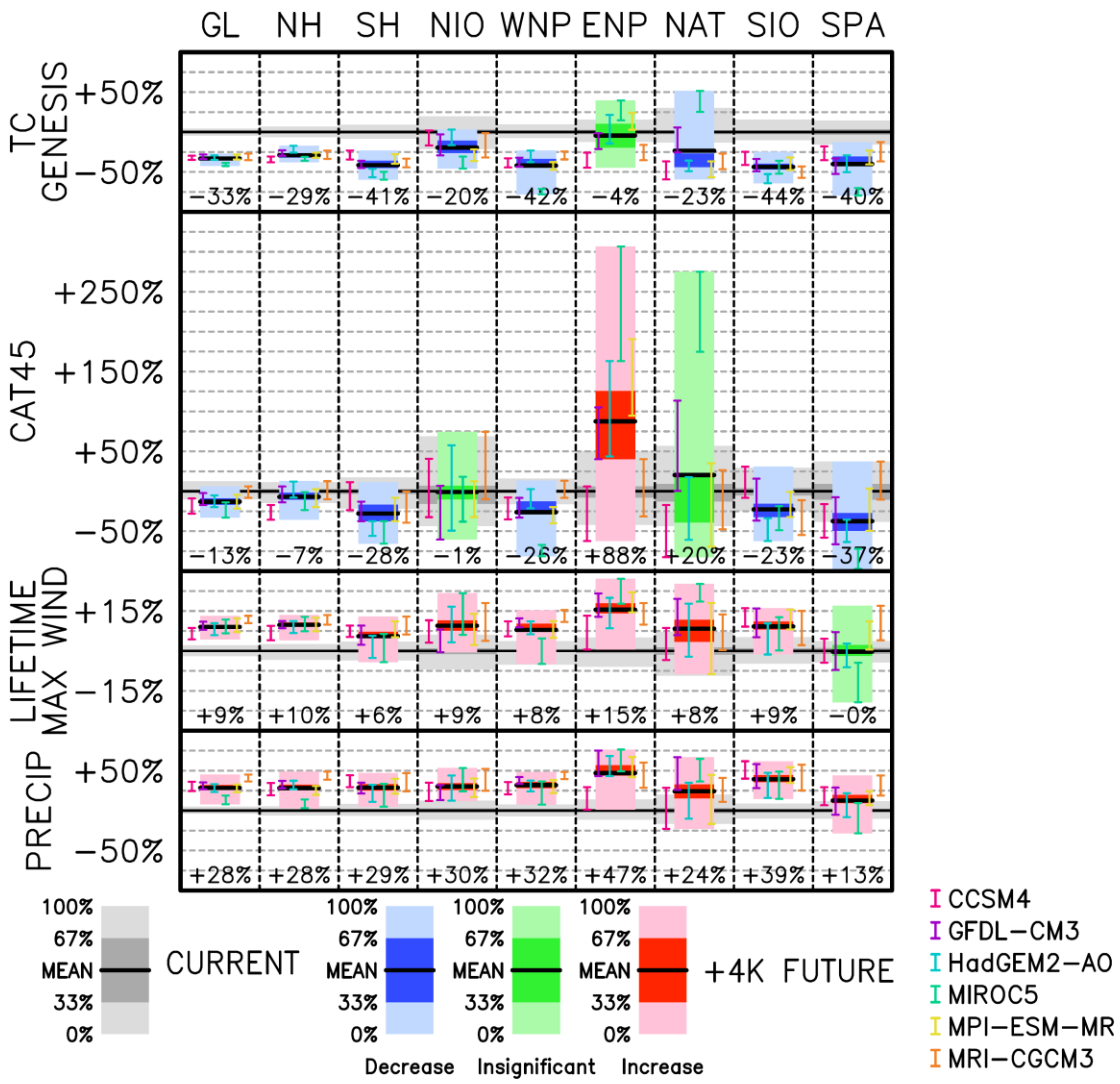

Figure S4. Same as Figure 4 but including uncertainty range for each SST warming pattern. See Table S1 for further details.

	SST	Global	NH	SH	NIO	WNP	ENP	NAT	SIO	SPA
Genesis frequency	6 CMIP5 models	**-33**	**-29**	**-41**	**-20**	**-42**	-4	**-23**	**-44**	**-40**
	(n=90 min/max)	(-43,-27)	(-38,-17)	(-60,-23)	(-46,3)	(-78,-23)	(-45,40)	(-59,52)	(-64,-25)	(-79,-13)
	CCSM4	**-33**	**-34**	**-29**	**-8**	**-37**	**-33**	**-48**	**-32**	**-28**
	(n=15 min/max)	(-35,-30)	(-38,-31)	(-34,-23)	(-17, 2)	(-44,-33)	(-45,-26)	(-59,-37)	(-41, -25)	(-35,-18)
	GFDL-CM3	**-31**	**-26**	**-40**	**-18**	**-37**	**-14**	**-9**	**-41**	**-42**
	(n=15 min/max)	(-34,-28)	(-30,-23)	(-45,-36)	(-29,-3)	(-43,-32)	(-21,-2)	(-25,6)	(-49, -34)	(-53,-33)
	HadGEM2-AO	**-32**	**-22**	**-52**	-8	**-31**	5	**-42**	**-58**	**-43**
	(n=15 min/max)	(-35,-29)	(-26,-17)	(-57,-46)	(-16, 3)	(-38,-23)	(-14, 21)	(-49,-36)	(-64, -53)	(-50,-29)
	MIROC5	**-41**	**-33**	**-55**	**-38**	**-74**	**29**	**41**	**-44**	**-74**
	(n=15 min/max)	(-43,-39)	(-36,-31)	(-60, -50)	(-46,-31)	(-78,-71)	(15,40)	(25,52)	(-52, -36)	(-79,-70)
	MPI-ESM-MR	**-31**	**-29**	**-34**	**-31**	**-43**	**15**	**-45**	**-39**	**-29**
	(n=15 min/max)	(-34,-28)	(-32,-26)	(-40,-28)	(-36, -22)	(-47,-38)	(3,24)	(-57,-37)	(-48,-32)	(-41,-23)
	MRI-CGCM3	**-32**	**-29**	**-38**	**-14**	**-30**	**-27**	**-37**	**-49**	**-24**
	(n=15 min/max)	(-35,-27)	(-34,-23)	(-44,-33)	(-32, -1)	(-34,-24)	(-35,-16)	(-47,-27)	(-57, -43)	(-37,-13)
Number of CAT45 TC	6 CMIP5 models	**-13**	**-7**	**-28**	-1	**-26**	**88**	20	**-23**	**-37**
	(n=90 min/max)	(-33,6)	(-36,13)	(-66,11)	(-61,75)	(-81,13)	(-62,307)	(-83,275)	(-62,31)	(-97,37)
	CCSM4	**-18**	**-23**	**-7**	4	**-22**	-32	**-44**	7	**-32**
	(n=15 min/max)	(-28,-9)	(-36,-17)	(-24,11)	(-32, 41)	(-35,-8)	(-62,6)	(-83,-17)	(-8,31)	(-58,-16)
	GFDL-CM3	**-10**	-4	**-25**	-24	**-20**	**72**	40	**-15**	**-43**
	(n=15 min/max)	(-17,-2)	(-14,6)	(-37,-13)	(-61, 7)	(-33,-8)	(40,105)	(0,114)	(-37,16)	(-66,-8)
	HadGEM2-AO	**-12**	2	**-48**	15	-13	**106**	-23	**-48**	**-49**
	(n=15 min/max)	(-20,-5)	(-8,12)	(-56,-37)	(-49,58)	(-21,3)	(44,163)	(-61,18)	(-62,-34)	(-64,-36)
	MIROC5	**-23**	**-10**	**-55**	-14	**-76**	**223**	**216**	**-37**	**-89**
	(n=15 min/max)	(-33,-14)	(-23,-1)	(-66, -37)	(-38, 18)	(-81,-67)	(163,307)	(175,275)	(-49,-19)	(-97,-72)
	MPI-ESM-MR	**-13**	**-9**	**-21**	-11	**-30**	**146**	-44	**-17**	**-27**
	(n=15 min/max)	(-22,-5)	(-20,3)	(-37, -8)	(-32, 13)	(-40,-20)	(95,190)	(-69, 35)	(-32,-1)	(-50,4)
	MRI-CGCM3	-2	3	**-12**	25	2	10	-22	**-27**	15
	(n=15 min/max)	(-8,6)	(-10,13)	(-39,0)	(-10,75)	(-8,13)	(-32,40)	(-48,26)	(-55,-11)	(-10,37)
Lifetime max surface wind	6 CMIP5 models	**9**	**10**	**6**	**9**	**8**	**15**	**8**	**9**	0
	(n=90 min/max)	(4,13)	(4,13)	(-4,13)	(2,22)	(-5,15)	(1,27)	(-9,25)	(-1,16)	(-19,17)
	CCSM4	**7**	**7**	**7**	**8**	**8**	**7**	**3**	**12**	-1
	(n=15 min/max)	(4,9)	(4,9)	(5,10)	(3,12)	(5, 11)	(1,13)	(-3,9)	(9,16)	(-4,5)
	GFDL-CM3	**9**	**10**	**6**	**4**	**10**	**17**	**12**	**10**	-1
	(n=15 min/max)	(8,11)	(9,11)	(2,9)	(0,8)	(9,12)	(13,22)	(6,20)	(5,16)	(-7,7)
	HadGEM2-AO	**8**	**9**	**2**	**11**	**8**	**15**	**6**	**6**	-1
	(n=15 min/max)	(6,10)	(7,11)	(-3,6)	(3,17)	(6,11)	(8,20)	(-2,18)	(-1,10)	(-6,3)
	MIROC5	**9**	**10**	1	**13**	-1	**22**	**21**	**6**	**-14**
	(n=15 min/max)	(7,12)	(7,13)	(-4,6)	(6,22)	(-5,5)	(18,27)	(19,25)	(0,13)	(-19,-4)
	MPI-ESM-MR	**9**	**10**	**8**	**9**	**9**	**18**	1	**11**	**4**
	(n=15 min/max)	(7,12)	(7,12)	(5,11)	(2,14)	(5,11)	(15,22)	(-9,18)	(8,15)	(1,11)
	MRI-CGCM3	**12**	**12**	**10**	**12**	**13**	**13**	**6**	**10**	**10**
	(n=15 min/max)	(10,13)	(10,13)	(6,13)	(4, 8)	(11,15)	(10,18)	(0,14)	(2,15)	(4,17)
Lifetime max precipitation rate	6 CMIP5 models	**28**	**28**	**29**	**30**	**32**	**47**	**24**	**39**	**13**
	(n=90 min/max)	(8,45)	(3,49)	(5,47)	(12,53)	(7,48)	(1,76)	(-23,67)	(15,62)	(-28,44)
	CCSM4	**30**	**27**	**36**	**23**	**29**	**15**	6	**49**	**18**
	(n=15 min/max)	(24,36)	(19,35)	(29,44)	(12, 35)	(20,36)	(1,29)	(-23,29)	(40, 62)	(7,29)
	GFDL-CM3	**32**	**33**	**29**	**24**	**38**	**55**	**39**	**42**	**11**
	(n=15 min/max)	(27,35)	(28,37)	(21,35)	(13, 32)	(33,42)	(43,75)	(26,67)	(28,58)	(-5,29)
	HadGEM2-AO	**28**	**30**	**21**	**28**	**30**	**58**	8	**32**	**10**
	(n=15 min/max)	(23,33)	(27,37)	(11,32)	(12, 44)	(24,37)	(43,68)	(-10,35)	(16, 47)	(-8,22)
	MIROC5	**13**	**11**	**19**	**38**	**19**	**62**	**51**	**30**	**-12**
	(n=15 min/max)	(8,19)	(3,14)	(5,34)	(24, 53)	(7,36)	(49,76)	(36, 65)	(15, 49)	(-28,10)
	MPI-ESM-MR	**27**	**26**	**30**	**32**	**31**	**54**	**13**	**41**	**16**
	(n=15 min/max)	(23,33)	(20,31)	(21,40)	(17, 40)	(22,38)	(42,67)	(-17,45)	(34, 54)	(7,24)
	MRI-CGCM3	**40**	**42**	**37**	**35**	**44**	**39**	**28**	**42**	**33**
	(n=15 min/max)	(37,45)	(39,49)	(24,47)	(25,52)	(39,48)	(29, 60)	(11,41)	(25, 58)	(19, 44)

Table S1. Future percent changes of the TC metrics to the climatological mean in the current climate simulations for the global ocean, the two hemispheres and individual ocean basins. TC metrics consist of TC genesis frequency, the number of TCs for CAT45 (≥ 59 m/s maximum surface wind speed), lifetime maximum intensity (LMI) of surface wind, and LMI of precipitation rate averaged within 200 km of the TC center. Shown are percent changes of the ensemble mean, minimum, and maximum values

among all ensemble members. Values of n indicate the number of the ensemble members. Bold letters indicate that the change is statistically significant.